Collagen and Leather

RESEARCH

Open Access

Cross-linking porcine peritoneum by oxidized konjac glucomannan: a novel method to improve the properties of cardiovascular substitute material

Xu Peng[1,2], Li Li[3], Jiaqi Xing[4], Can Cheng[1], Mengyue Hu[1], Yihao Luo[1], Shubin Shi[1], Yan Liu[2], Zhihui Cui[5] and Xixun Yu[1*]

Abstract

The use of natural polysaccharide crosslinkers for decellularized matrices is an effective approach to prepare cardiovascular substitute materials. In this research, $NaIO_4$ was applied to oxidize konjac glucomannan to prepare the polysaccharide crosslinker oxidized konjac glucomannan (OKGM). The as-prepared crosslinker was then used to stabilize collagen-rich decellularized porcine peritoneum (DPP) to construct a cardiovascular substitute material (OKGM-fixed DPP). The results demonstrated that compared with GA-fixed DPP and GNP-fixed DPP, 3.75% OKGM [1:1.5 (KGM: $NaIO_4$)]-fixed DPP demonstrated suitable mechanical properties, as well as good hemocompatibility, excellent anti-calcification capability, and anti-enzymolysis in vitro. Furthermore, 3.75% OKGM [1:1.5 (KGM: $NaIO_4$)]-fixed DPP was suitable for vascular endothelial cell adhesion and rapid proliferation, and a single layer of endothelial cells was formed on the fifth day of culture. The in vivo experimental results also showed excellent histocompatibility. The current results demonstrted that OKGM was a novel polysaccharide cross-linking reagent for crosslinking natural tissues featured with rich collagen content, and 3.75% OKGM [1:1.5 (KGM: $NaIO_4$)]-fixed DPP was a potential cardiovascular substitute material.

Keywords Sodium periodate, Oxidized KGM, Peritoneum, Collagen, Cardiovascular substitute material

*Correspondence:
Xixun Yu
yuxixun@163.com
Full list of author information is available at the end of the article

Graphical Abstract

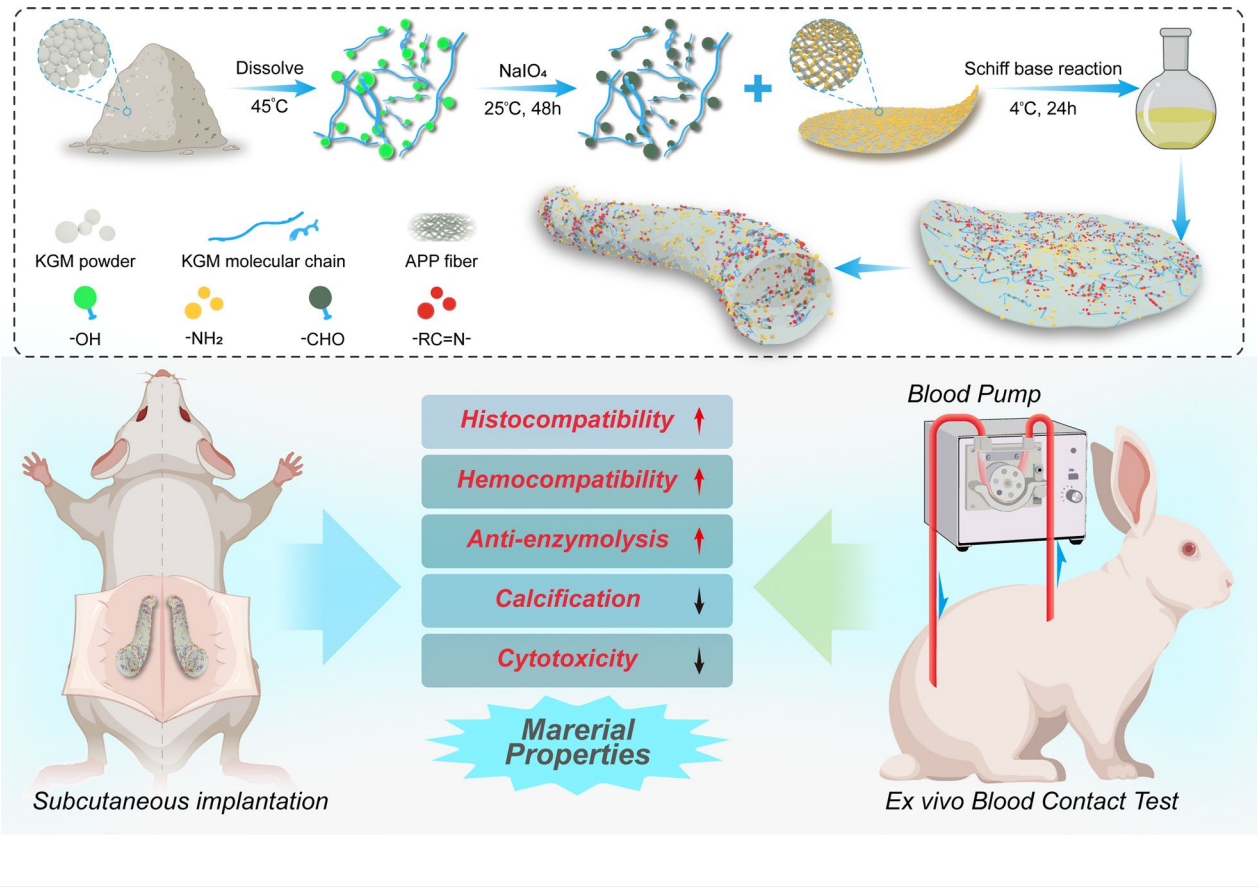

1 Introduction

Heterogeneous decellularized tissues have been widely used in the preparation of vascular grafts because their construction is suitable for cell adhesion, proliferation, and migration. The products currently developed include the Artegraft bovine common carotid artery [1], ProCol bovine mesenteric vein [2, 3], and Synergraft bovine ureter [4]. However, some decellularized tissues have not been used clinically, including the human umbilical vein, porcine carotid artery, porcine saphenous artery, and other acellular matrices. All the decellularized scaffolds were rich in collagen and elastin. Elastin is the main extracellular matrix component of vascular tissues. Lack of elastin can lead to failure of blood vessels, including aneurysms, thrombosis, and intimal hyperplasia [5–8]. The peritoneum of the Bama pig is also a tissue rich in elastin and is easier to obtain than other tissues. The peritoneum, rich in blood capillaries, lymphatic vessels, and nerves, exhibits flexibility and a smooth surface. The peritoneum has the same embryologic origin as blood vessels and a low risk of thrombosis. Additionally, the Bama pig peritoneum demonstrates desired permeability along with a certain degree of regenerative properties, adequate mechanical properties, and a thickness similar to that of the 2 mm diameter-natural vessels (300–500 μm). Therefore, it is suitable for use in preparing artificial vessels with diameters of 2 mm.

However, the direct application of porcine peritoneum onto the construction of replacement grafts can cause immune rejection. DPP can greatly reduce its immunogenicity, but its poor mechanical properties and stability in physiological environments prevent its direct use or preservation. Therefore, the pre-fixation of these animal-derived decellularized tissues is required to address these problems [9]. Glutaraldehyde (GA), the most common crosslinking agent used for pre-fixation, can enhance the biomechanical properties of acellular tissues and improve their stability. However, as many researchers have confirmed, the application of Glutaric dialdehyde (GA) is limited by calcification and cytotoxicity as well as the inability to crosslink elastin

[10]. Genipin (GNP) is an excellent, naturally occurring crosslinking agent that has been developed in recent years. Its cytotoxicity is lower than that of GA alone. However, the color of tissues crosslinked by GNP is dark blue, and the thickness of GNP-fixed tissues increases excessively [11]. These shortcomings restrict the further application of GNP. There is an urgent need to find a suitable crosslinking agent to pre-fix acellular tissues to improve their mechanical properties, further reduce their antigenicity, and enhance their resistance to enzymatic degradation while maintaining their original ultrastructure.

Konjac glucomannan (KGM) is a high-molecular-weight, water-soluble, non-ionic natural polysaccharide. It exhibits good biocompatibility, biodegradability, and excellent gel-forming properties and is used in cosmetics, drug-controlled release materials, and plasma substitutes. KGM is linked by β-1,4 glycosidic bonds and is rich in hydroxyl groups, providing opportunities for this polysaccharide to be modified for other biomedical applications. The *o*-hydroxyl groups of KGM can be selectively oxidized by sodium periodate ($NaIO_4$) into aldehyde groups, yielding oxidized KGM (OKGM) with multiple functional aldehyde groups. OKGM can bridge amine groups in heterogeneously derived acellular tissues through reactive formyl-aldehyde groups to form a stable cross-linking structure [12–14].

This research evaluated various physical and chemical properties of OKGM-fixed DPP, including its ultrastructure, mechanical properties, stability, cytocompatibility, hemocompatibility, in vitro calcification, and in vivo inflammation. This research first provides an experimental basis for OKGM as a new cross-linking reagent for fixing natural tissues featured with rich collagen content.

2 Materials and methods

2.1 Preparation and characterization of OKGM

After 5 g of KGM (K8170, Solarbio) was dissolved in 500 mL distilled water, 7.5 g of $NaIO_4$ (S817518, Solarbio) was added to the KGM solution. The oxidation reaction proceeded in the dark at room temperature for 48 h. Subsequently, 20 mL ethylene glycol was added to the mixture to remove excess $NaIO_4$. Crude OKGM was obtained via precipitation with excess ethanol and suction filtration. Finally, the obtained OKGM was immediately dialyzed (with a molecular weight cutoff of 3000) with deionized water for 3 days and subsequently lyophilized using a vacuum freeze dryer to obtain purified OKGM.

The aldehyde content of OKGM was determined by the potentiometric titration of hydroxylamine hydrochloride. The weight-average molecular weight (Mw), number-average molecular weight (Mn), and polydispersity (Mw/Mn) of OKGM were determined using aqueous gel permeation chromatography (Waters 1515). Zeta potential (ζ) measurements of products were analyzed in a Malvern Zeta sizer (Nano Model ZS90) at a constant temperature of 25 °C. For the FTIR measurement of OKGM, 4 mg of dry samples and 40 mg of KBr were pressed into a disc. A Nicolet 560 infrared spectrometer was used to measure the FTIR spectra at a resolution of 4 cm^{-1} in the wavenumber range of 400–4000 cm^{-1}.

2.2 Preparation of DPP and fixation index of OKGM-fixed DPP

The fresh peritoneum was immersed in 1% Triton X-100/deionized water and 0.5% SDS/deionized water and shaken (60 rpm) for 3 h. Subsequently, the samples were soaked while undergoing continuous magnetic mechanical stirring for 3 h. Finally, the samples were washed several times with PBS to remove cellular remnants. DNase I (200 U/mL) was used to treat samples at 37 °C for 4 h. DPP was obtained using the decellularization process described above.

DPPs were immersed in a series of OKGM/PBS solutions with different OKGM concentrations (3.75, 7.5, and 15% m/v) to fix the samples. The DPPs were all fixed at 37 °C for 24 h in a constant temperature oscillator.

At predetermined times, all the OKGM-fixed DPPs were lyophilized for at least 12 h to a constant weight. After heating the NHN solution to boiling for 20 min, lyophilized tissues were removed, and the optical absorbance of the solution was measured using an enzyme-labeled instrument (Multiskan FC, Thermo Fisher) at 570 nm. Glycine at various known concentrations was used as the standard, and the fixation index (FI) was calculated using the following formula:

$$FI\% = \frac{(NHNreactive\ amine)_{fresh} - (NHNreactive\ amine)_{fixed}}{(NHNreactive\ amine)_{fresh}}$$

2.3 Surface characterization of samples

Field-emission scanning electron microscopy (FE-SEM, Oberkochen) was used to evaluate the surface topographies of the samples. The hydrophilicity of the surfaces of the samples (lyophilized 2.5 cm × 2.5 cm) was characterized by a water contact angle goniometer (WCA, SL200KS).

2.4 Cytocompatibility and in vitro endothelialization of OKGM-fixed DPP

Human vascular endothelial cells (HVEC, purchased from the Lab of Transplant Immunology West China Hospital) were inoculated with 1×10^5 cells/mL on Co-60 irradiated sterilized samples (2 cm × 2 cm) in

6-well culture plates. DMEM (2000 μL with 10% FBS) was added after 30 min. The culture medium was changed every two days. CCK8 (Cell Counting Kit-8, Beyotime) assays were performed on days 1, 3, and 5. Cell live/dead fluorescent staining (Calcein AM, Beyotime) was performed on day 2 to observe cell adhesion and activity on the surface of the sample. SEM was used to observe HVEC attachment morphology on sterilized samples after incubation for 3 days. After the fifth day of culturing, the cell sample constructs were washed with PBS, fixed with paraformaldehyde, and stained with HE to observe the endothelialization of OKGM-fixed DPP in vitro.

2.5 Hemocompatibility measurement

2.5.1 Hemolytic test

Red blood cell (RBCs) separation 10 mL of rabbit blood anticoagulated with sodium citrate were added to 20 mL DPBS to ensure uniform dispersion. The RBCs were separated by centrifugation at 500 × g for 10 min. Thereafter, the RBCs were rinsed with DPBS several times and re-suspended in 100 mL DPBS solution. RBCs dispersed in DPBS were used as negative controls, while those dispersed in distilled water were used as positive controls.

Gradient concentration hemolysis test All OKGM-fixed DPP samples were ground to powders and dispersed in PBS at gradient concentrations to form a suspension. 0.4 mL of RBC solution was then added to 1.6 mL suspensions at each concentration soon afterward, and all mixtures were incubated for 3 h at 37 °C.

Direct contact hemolysis test The sample was cut into 2 cm × 2 cm pieces and placed flat in a 6-well plate. Then, 2 mL of RBC suspension was added to each well, and the samples were incubated for 3 h at 37 °C.

The suspension was centrifuged, and the absorbance of the supernatant was measured at 540 nm. The hemolysis rate (%) was calculated as follows:

$$\begin{aligned}\text{Hemolysis rate (\%)} &= (\text{experimental group} - \text{negative control group}) \\ &/(\text{positive control group} - \text{negative control group}) \\ &\times 100\end{aligned}$$

2.5.2 Static platelet adhesion test

Whole blood was centrifuged (1000 r/min for 10 min) to separate platelet-rich plasma (PRP). 400 μL of PRP was dropwise added on the surface of DPP-samples, which have been pre-immersed and equilibrated in PBS at 37 °C for at least 1 h. Then, they were incubated at 37 °C for 1 h. These DPP-samples were mildly washed with PBS to remove non-adherent platelets before being fixed with a 2.5% GA/PBS solution for 8 h at 4 °C. Finally, the DPP-samples were dehydrated using gradient ethanol (50, 70, 85, 90, 95, and 100%) for 10 min per concentration, and the morphology and aggregation of the attached platelets were observed using SEM.

2.5.3 Ex vivo blood contact test

The DPP-samples were cut into square patches (4 mm × 9 mm) and pre-immersed in PBS for 1 h. The patches were then attached to the internal walls of silicone tubes (ID = 3.1 mm) pre-soaked with heparin. General anesthesia of experimental rabbits weighing 3 kg each was induced through the intravenous administration of 10 mg/kg pentobarbital sodium salt (Sigma, 57-33-0). 40 μg/kg of the sedative dexmedetomidine hydrochloride (Zoetis, 1852761) was also administered intravenously. 0.3 mg/kg Butorphanol (MSD, A141A04) for preemptive analgesia was administered intramuscularly.

After opening the abdominal cavity from the midline, 2 cm of the abdominal aorta was separated and exposed. The vessel was clamped using arterial clamps at the distal and proximal ends. Next, the artery was cut from the middle, and the vascular stump was flushed with heparinized saline. A cannula (0.8 mm × 1.6 mm) was inserted into the vascular stump and bound using sutures to prevent cannula dislodgement. Blood was collected from the proximal arterial drainage tube and infused into degassed sample tubes to interact with the materials using peristaltic pumps (YZ1515x, Longer). Blood was then injected into the distal arterial drainage tube to complete circulation. The infusion lasted for 2 h. After completing the perfusion procedure, the DPP-samples were removed, fixed with 2.5% GA solution, and observed using SEM.

2.6 Enzymatic hydrolytic resistance

After being lyophilized to constant weight, all samples were immersed into 1.5 mL collagenase I/PBS (S10053, Yuanye Shanghai) (25 U/mL), collagenase IV/PBS (S10056, Yuanye Shanghai) solutions (25 U/mL), Elastase/PBS (S10165, Yuanye Shanghai) solutions (25 U/mL), respectively, and incubated at 37 °C with constant shaking. The samples were then transferred to a 10 mM EDTA solution to terminate the enzymatic hydrolysis reaction at predetermined time points (0.5, 1, 3, 6, 12, 24, 48, and 72 h). The enzymatically hydrolyzed samples were lyophilized and weighed. The percentage of weight loss ($\Delta W\%$) was calculated using the following formula:

$$\Delta W\% = \frac{W_0 - W_t}{W_0} \times 100\%$$

W_0 represents the initial weight before degradation, and W_t represents the weight of the corresponding sample after degradation.

2.7 In vitro calcification

The lyophilized and sterilized 1 cm × 1 cm samples were immersed in 2 mL of simulated body fluid (SBF, JISS-KANG) and incubated in a constant temperature incubator at 37 °C. The SBF was changed weekly and the entire process remained aseptic. The samples were collected and washed with distilled water at pre-determined times (after 30, 60, and 90 d). After dehydration by gradient alcohol and drying at the critical point of CO_2, the surfaces of the samples were observed by SEM, and the surface calcium content of the samples was detected using EDS.

2.8 Mechanical properties

2.8.1 Uniaxial tensile test

The samples were investigated before and after fixation to determine if any improvement in the biomechanical properties could be detected. The samples were cut into rectangular strips of 40 mm × 10 mm, and their thicknesses were measured by a micrometer. Uniaxial tensile tests were performed using an Instron material testing machine (Instron Co., USA) at an extension rate of 7 mm/min. The ultimate tensile strain and the ultimate tensile stress were recorded when the sample was torn. The ultimate elastic modulus was determined from the ultimate tensile stress–strain curve.

2.8.2 Suture retention strength

The suture retention test was performed according to the American National Standard Institute /Association for the Advancement of Medical Instruments (ANSI/AAMI) VP20 standard. Each sample was cut into rectangular strips (40 mm × 10 mm). A single 5–0 absorbable suture loop was created 2 mm away from the sample edge and secured to a hook connected to the clamp of the testing device. The suture retention strength was defined as the maximum force recorded at an extension rate of 7 mm/min when the sample was torn. Suture retention tension was obtained by normalizing the suture retention strength to the thickness of each sample.

2.9 Subcutaneous implantation

Subcutaneous implantation in rats is the standard FDA-accepted technique for evaluating cardiovascular materials. SD rats were purchased from Chengdu Dossy Experimental Animals CO, Ltd. Rats were inhalation anesthetized with of 1–2% isoflurane gas, and sterilized DPP-samples were implanted subcutaneously on both sides of their backs. After recovery from anesthesia, all rats were fed a standard diet. Rats were euthanized with excess isoflurane gas after 90 days, and each collected implantation sample was fixed in 4% formaldehyde for HE staining analysis.

2.9.1 Statistical analysis

Data are expressed as mean ± standard deviation and were analyzed by one-way ANOVA using SPSS (version 20.0), $p < 0.05$.

3 Results and analysis

3.1 Preparation and characterization of OKGM

3.1.1 Oxidation degree, molecular weight, and polydispersity of OKGMs prepared with different feeding ratios of KGM/$NaIO_4$

With the increase in $NaIO_4$, the Mn and Mw of OKGM showed a downward trend, and the aldehyde group content within OKGM increased because of the breaking of the polysaccharide chain (Table 1). The molecular weights and physiological activities of the crosslinking agents are different. OKGM with a large molecular weight has both low cytotoxicity and low crosslinking properties owing to its better diffusion and ability to reach more reaction sites to react with the amino groups within the tissue. In addition, the molecular weight of the crosslinking agent has an important relationship with its metabolic time in vivo. The larger the molecular weight of OKGM, the more complex its structure and the more difficult it is for OKGM in vivo [15, 16]. Therefore, appropriate $NaIO_4$ consumption is key to the preparation of OKGM. According to the pre-experiment, we selected three OKGM samples prepared with different feeding ratios of KGM/$NaIO_4$ (mass ratios of KGM/$NaIO_4$ were 1:1, 1:1.5, and 1:2) to further investigate their crosslinking properties and the physicochemical and biological properties of OKGM-fixed samples to ascertain the best

Table 1 Oxidation degree, molecular weight, and polydispersity of various OKGMs

KGM/$NaIO_4$ mass ratios	Oxidation degree	Number-average Molecular Weight	Mass average molar mass	Mw/Mn
1:1	21% ± 2.3%	3623	15,310	4.23
1:1.5	32% ± 1.8%	3001	7500	2.49
1:2	47% ± 1.7%	2534	7475	2.95

matching of KGM and $NaIO_4$ for preparing OKGM used as a crosslinking agent.

3.1.2 FTIR analysis of OKGM

OKGM was prepared by the $NaIO_4$ oxidation method (Fig. 1a). The presence of dialdehyde groups was verified by FTIR analysis. As shown in Fig. 1b, the spectrum of OKGM shows a new characteristic peak at 1727.5 cm^{-1}, which is the most characteristic band of the C=O vibrations of the aldehyde group. This peak clearly indicates the formation of active aldehyde groups in the OKGM molecular chain. A new infrared band at 892 cm^{-1} suggests the formation of hemiacetals between the aldehyde groups and non-oxidized hydroxyl groups. Therefore, the aldehyde group was successfully introduced through periodate oxidation.

3.1.3 Zeta potential of OKGM

The OKGMs with different degrees of oxidation presented different zeta potential values. This may be owing to the different types and numbers of functional groups on the surface of OKGMs. The higher the feeding ratio of $NaIO_4$, the higher thetable degree of oxidation of an OKGM (Table 2), and more aldehyde groups are formed in the OKGM molecular chain. Owing to the electronegativity of oxygen atoms in aldehyde groups, the electron cloud of the carbon–oxygen double bond will shift toward the oxygen atoms, eventually leading to an increase in the electronegativity of the overall system. This increase in polarity is manifested as an increase in the absolute value of the potential.

3.2 Decellularization of peritoneum and characterization of DPP

The fresh porcine peritoneum (FPP) is a semi-transparent film with a thickness of approximately 0.2–0.5 mm. After decellularization, the tissue thickness significantly increased to about 0.8 mm (Additional file 1: Fig. S1). Lyophilized DPP appeared as a white sheet with good flexibility, as shown in Fig. 2a.

Table 2 Zeta potential of OKGM

Material	Zeta potential (mV)
KGM	− 17.40
1:1 OKGM	− 20.76
1:1.5 OKGM	− 23.90
1:2 OKGM	− 25.97

3.2.1 Residual DNA of DPP

Residual cellular components in ECM can cause adverse host reactions in vivo and increase the risk of heterogeneous antigen transmission. Double-stranded DNA (dsDNA) can be quantitatively assessed as an indicator of cell residue in the ECM. Previous studies have suggested that the minimal standard concentration of dsDNA in the ECM is < 50 ng/mg. Our research demonstrates that the total DNA content of DPP is significantly decreased by 91.5% (44 ± 12 ng/mg) after decellularization when compared to that of FPP (519 ± 80 ng/mg) (Fig. 2c), which meets the standard of clinical application of ECM. DAPI staining of fresh and decellularized porcine peritoneum was also performed to determine the extent of DNA removal. As shown in Fig. 2b, the number of intact nuclei in the FPP is much higher than that in the DPP. Almost no nuclei are observed in the DPP. HE staining is a simple qualitative indicator used to observe whether tissues contain nuclei to confirm the removal of nucleic acids from tissues [17]. In this experiment, there are no residual cells with intact structures in the DPP fiber voids after decellularization, based on the HE staining results (Fig. 2e).

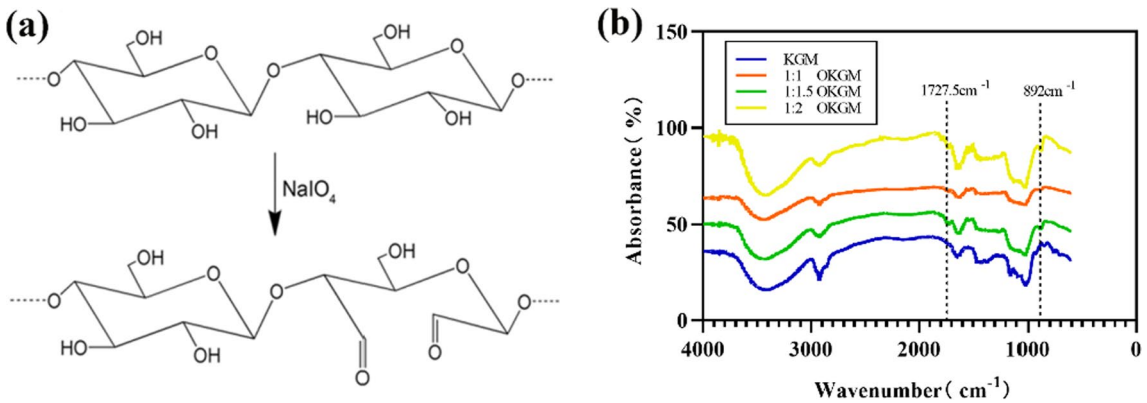

Fig. 1 Characterization of OKGM. **a** Schematic diagram of preparing OKGM. **b** FTIR analysis of OKGM

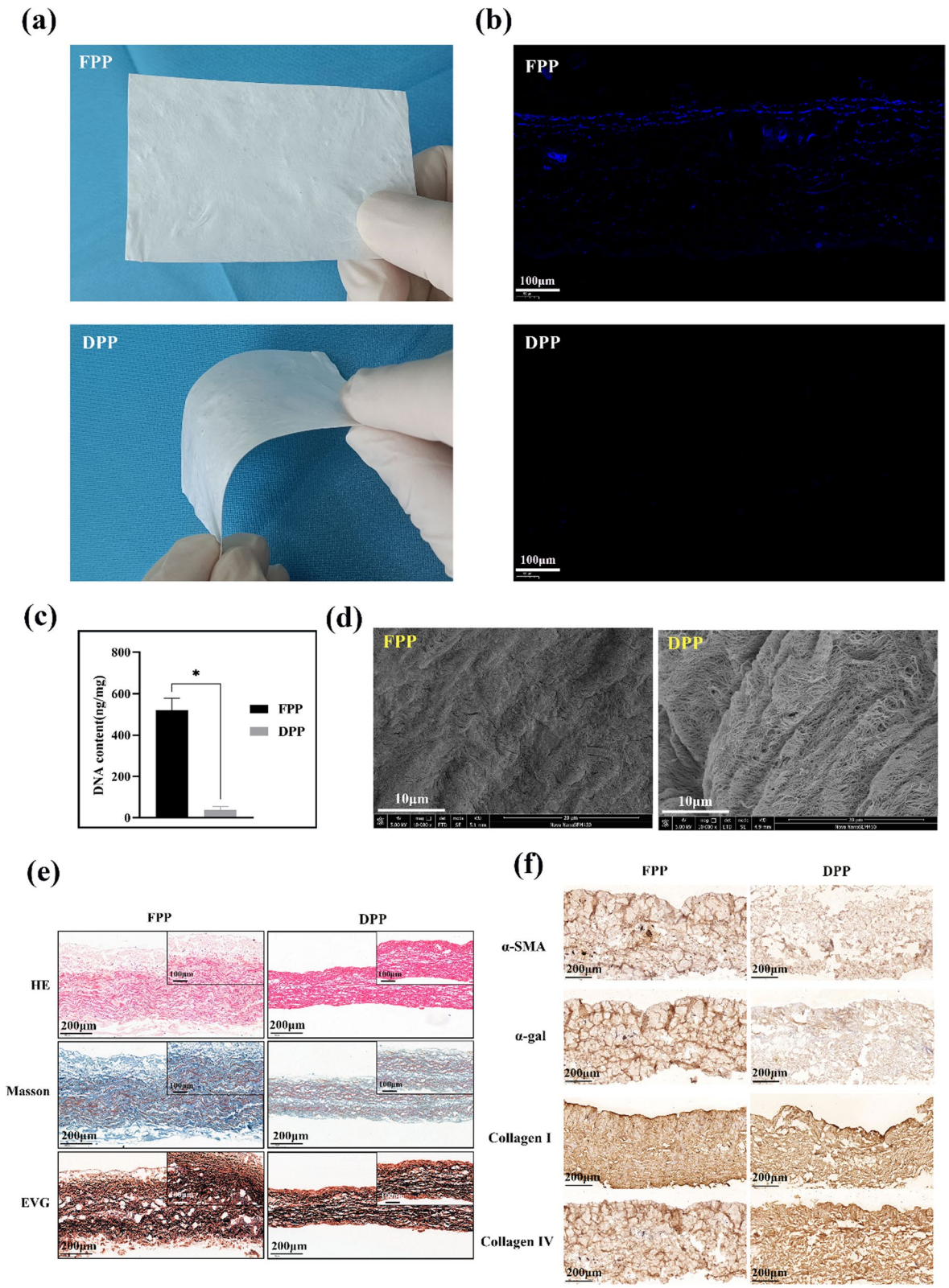

Fig. 2 Characterization of decellularized peritoneum. **a** Lyophilized DPP. **b** DAPI staining of FPP and DPP. **c** Residual DNA of DPP. **d** Microstructure of fiber in samples under SEM. **e** HE, Masson, EVG staining of collagen fibers, muscle fibers and elastic fibers in samples. **f** Expression of α-Gal, α-SMA, collagen I, collagen IV in samples

3.2.2 Ultrastructure of DPP and FPP

The SEM results (Fig. 2d) show that after decellularization, the fibers in the peritoneum became loose but less broken, and the directions of the fibers are similar. The results of HE, Masson, and EVG staining (Fig. 2f) show that collagen and elastic fibers remain intact after decellularization.

3.2.3 The expression level of α-Gal, α-SMA, collagen I and collagen IV in DPP

α-Gal is widely expressed in most mammalian tissues (including humans and higher primates), and α-Gal remaining in the cytomembrane can cause hyperacute immune rejection reactions after xenotransplantation [18, 19]. The absence of α-Gal could be considered a sign of successful decellularization. α-SMA is a marker protein of vascular smooth muscle, and its expression level can be used as an indicator of the degree of clearance of smooth muscle cells [20]. The weak expression of α-Gal and α-SMA (Fig. 2f) in DPP indicates the successful decellularization of FPP and the safety of this animal-derived substitutional material.

Collagen accounts for approximately one-third of the total proteins in all vertebrates. It is biodegradable with weak antigenicity and good biocompatibility [21]. However, after decellularization, its natural assembly structure is destroyed, resulting in decreased mechanical properties and stability. The results of collagen immunohistochemical staining (Fig. 2f) shows that the expression of type I and type IV collagen both in FPP or DPP is abundant and mainly concentrated in the basal layer [22, 23].

3.3 Preparation and characterization of OKGM-fixed DPP

After crosslinking with OKGM, GNP, and GA, it was found that GNP-fixed DPP becomes dark bluish, while the color of both GA-fixed and OKGM-fixed DPP turn yellow. The freeze-dried DPP-samples are shown in Fig. 3b.

3.3.1 The fixation of DPP by OKGM

The FI was used to quantitatively evaluate the degree of crosslinking. The results demonstrated that the FI of OKGM-fixed DPP was correlated with the feed ratio of KGM/$NaIO_4$ for preparing OKGM and the concentration of OKGM. As shown in Fig. 3a, the fixation of samples by 7.5 and 3.75% OKGM prepared with different feeding ratios of KGM/$NaIO_4$ (the mass ratio of KGM/$NaIO_4$ is 1:1, 1:1.5, 1:2) is stable, and after 24 h of fixation, their FI reaches a maximum (> 60%). There is no significant difference in FI during the entire course of the test between the 3.75 and 7.5% OKGM-fixed DPP.

Studies have reported that the degradation rate of decellularized tissue affects tissue regeneration after implantation [24]. The in vivo degradation rate of animal-derived scaffolds could be controlled by their FI. The 95%-FI bovine pericardium was more resistant to enzymatic degradation than its 60%-FI counterpart in research of GNP-fixed bovine pericardium [25]. Consequently, tissue regeneration was limited in the 95%-FI acellular tissue throughout the entire research (1 year post-operatively), whereas tissue regeneration was observed in the 60%-FI acellular tissue [26]. In conclusion, FI determines the degradation rate of acellular tissue and its regeneration pattern. Therefore an appropriate FI ($\geq$ 60%) should be taken into account the ability to resist enzymolysis and tissue regeneration.

Based on the principles of easy dissolution, short fixation time, and stable FI, the following three conditions: (1) 1:1, 3.75%, 24 h; (2) 1:1.5, 3.75%, 24 h; and (3) 1:2, 3.75%, 24 h, were initially selected to prepare OKGM, and the prepared OKGM was further used for the following experiment.

3.3.2 Water contact angle

Appropriate surface hydrophilicity is a prerequisite and a basis for good cytocompatibility of biomaterials. Superhydrophilic or superhydrophobic surfaces are not conducive to cell spreading and adhesion. The water contact angle (WCA) of the DPP was approximately 77° (Fig. 3c). After crosslinking with GA and OKGM, the WCA of the fixed samples increased to 87.6° and 91.1°, respectively. This may be because of the massive consumption of amino groups on the surface of DPP by GA or OKGM, leading to a weakened interaction force between the fixed sample and the water droplet. Therefore, the surfaces of DPP fixed with GA or OKGM exhibited slight hydrophobicity compared to that of DPP alone. After crosslinking with GNP, the WCA of the fixed samples decreased significantly to 14.1°. This might be because a large number of amino groups remained on the DPP surface due to the different crosslinking mechanisms of GNP. Moreover, the carboxyl and hydroxyl groups on the GNP were exposed. All these events resulted in a reduction in WCA. The surfaces of GA-fixed DPP and OKGM-fixed DPP are neither too hydrophilic nor too hydrophobic, which could effectively promote cell adhesion and spreading.

3.3.3 The fiber structure of fixed DPP

After crosslinking with GA and GNP, the DPP fibers exhibited anisotropic characteristics (Fig. 3d). The fibers

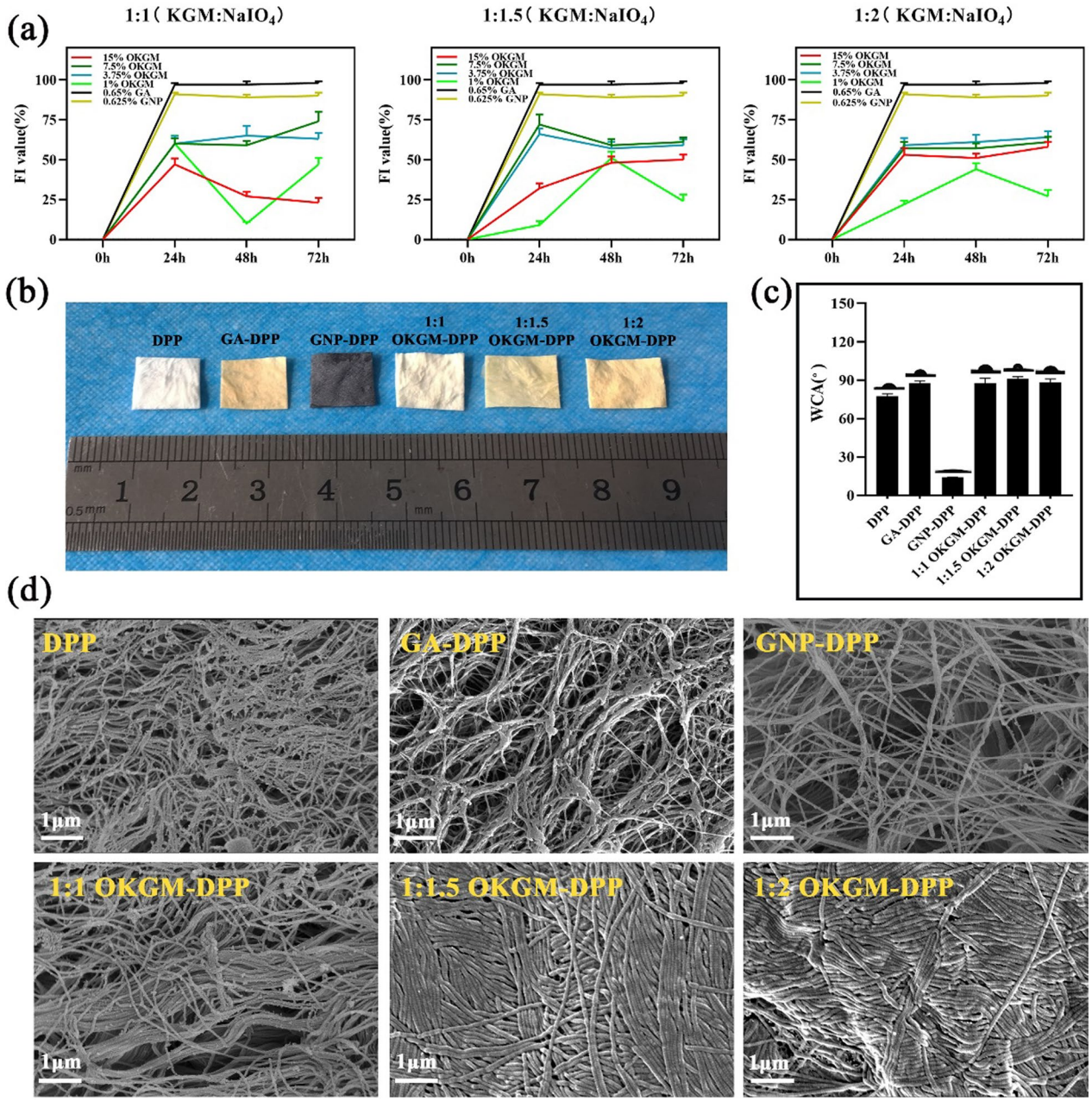

Fig. 3 Characterization of fixation and water contact angle. **a** Influence of different oxidation degree, concentration, and crosslinking time of OKGM on the fixation of samples. **b** Preparation of OKGM-fixed DPP (from left to right is DPP, GA-fixed DPP, GNP-fixed DPP and DPPs crosslinked with various OKGM prepared with different feeding ratios of KGM/$NaIO_4$ (the mass ratio of KGM/$NaIO_4$ is 1: 1, 1:1.5, 1:2). **c** Water contact angle. **d** Fiber structure of fixed DPP

in the GA-fixed DPP were tighter than those in the GNP-fixed DPP. For OKGM-fixed DPP, with the increase in $NaIO_4$ concentration, the aldehyde group content within OKGM (the oxidation of OKGM) increased, the structures of the fibers were more compact, and the fiber orientation was basically the same. This indicated that the cross-linking by OKGM did not destroy the original structure of the fiber but rather made the fiber structure denser.

3.4 Cytocompatibility and in vitro endothelialization of OKGM-fixed DPP

The lumen surface of a vascular graft can trigger thrombosis owing to the deposition of platelets. The absence or

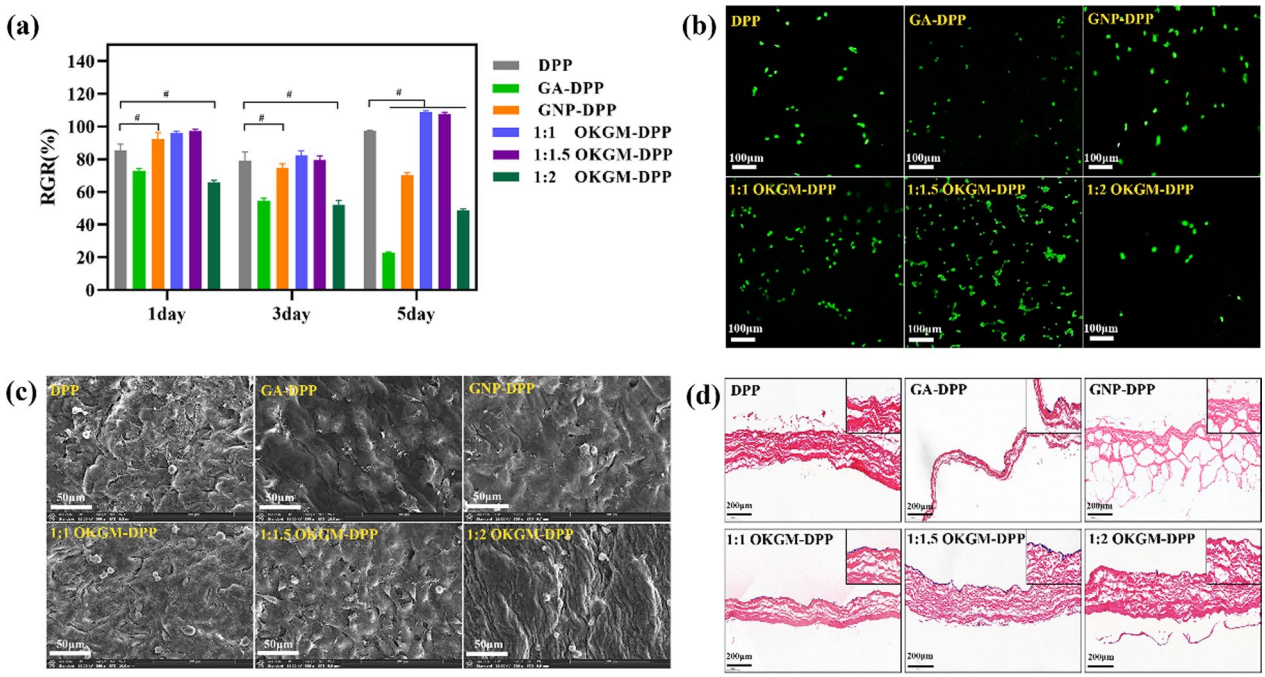

Fig. 4 Cytocompatibility and in vitro endothelialization of OKGM crosslinked DPP. **a** HEVCs-cytocompatibility of fixed DPP (# means significant difference compared with DPP group). **b** Live/dead cell fluorescent staining image of HUEVCs on samples on the second day. **c** HUEVCs adhered on fixed DPP on the third day. **d** Proliferation and endothelialization of HUEVCs on samples on the fifth day

delay of endothelialization and the migration and proliferation of smooth muscle cells (SMC) on the lumen surface of vascular grafts can lead to intimal hyperplasia [27]. Re-endothelialization is the first key point in inhibiting intimal hyperplasia and thrombosis. A completely spread monolayer of endothelial cells can ensure normal blood flow and the functional expression of EC [28, 29].

After seeding HUEVCs on fixed DPP and culturing for 1, 3, and 5 days, the proliferation of HUEVCs was detected by CCK8 (Fig. 4a). The adhesion of HUEVCs on the second and third days was detected by live/dead cell fluorescence staining (Fig. 4b) and SEM (Fig. 4c), respectively. The proliferation and endothelialization of HUEVCs on samples on the fifth day tested by HE staining (Fig. 4d). The results showed that the samples in the 1:1 OKGM-fixed and 1:1.5 OKGM-fixed groups had similar relative generation rates (RGR) of HUEVCs, basically maintaining around 70–90% within 5 days. This was significantly higher than that of the GA-, GNP-, and 1:2 OKGM-fixed DPP. Live/Dead cell fluorescence staining and SEM results showed that HUEVCs had good adhesion on the surface of 1:1 OKGM-fixed and 1:1.5 OKGM-fixed DPP, spreading fully with their characteristic fusiform morphology on sample surfaces. In contrast, the GA- and 1:2 OKGM-fixed samples showed a certain degree of cytotoxicity, with no obvious normal adhesion of HUEVCs on 1:2 OKGM-fixed DPP. As shown in Fig. 5d, compared with counterparts in other groups, significantly confluent monolayers are found on the surfaces of the 1:1 OKGM- and 1:1.5 OKGM-fixed DPP. The above results indicated that 1:1 OKGM- and 1:1.5 OKGM-fixed DPP presented low cytotoxicity and high HEVC cytocompatibility. This was partly because of the good biocompatibility of OKGM. Furthermore, OKGM could also crosslink collagen and elastin, which enhances the ability of OKGM-fixed DPP to resist enzymatic hydrolysis in vitro, avoiding the cytotoxicity resulting from the small molecule toxic substances produced by rapid degradation of samples in vitro. Conversely, the excessive aldehyde groups in the 1:2 OKGM-fixed DPP could result in some cytotoxicity.

3.5 Hemocompatibility of OKGM-fixed DPP

Hemocompatibility is the most important criterion for the successful application of cardiovascular substitute materials in vivo [30]. Figure 5a shows the hemolysis rate of various DPP-samples as a function of suspension concentration of the samples after incubation with RBCs at 37 °C for 3 h. As shown in the figure, the hemolysis rate of OKGM-fixed samples is lower than that of GA-fixed and GNP-fixed samples. In addition, the hemolysis rate is less than 5% for 1:1 and 1:1.5 OKGM-fixed samples at a concentration of 25 μg/mL, which was much higher than the concentration value that was possibly reached in vivo.

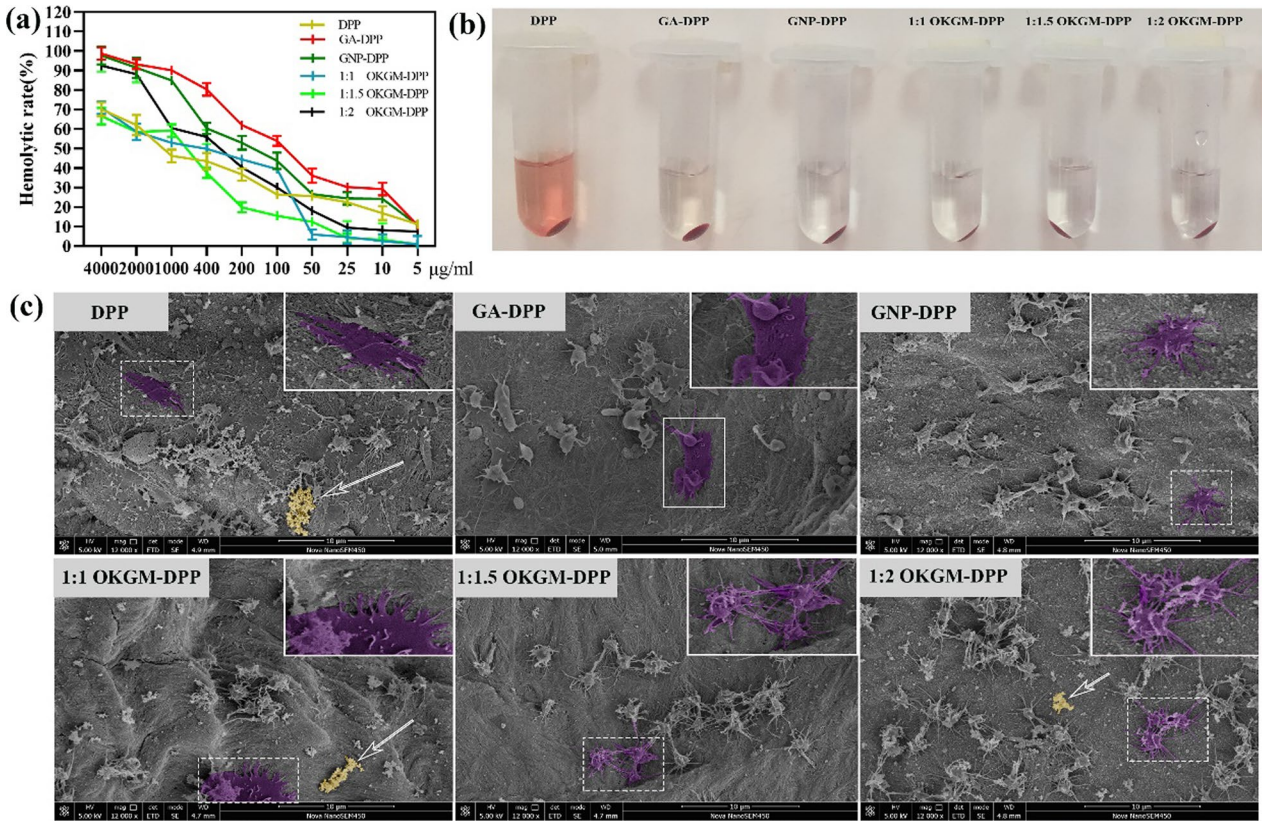

Fig. 5 Hemocompatibility and static platelet adhesion of OKGM-fixed DPP. **a** Hemolysis rate of various DPP-samples as a function of suspensions concentration of samples. **b** Complete DPP-samples direct contact hemolysis test. **c** Static platelet adhesion of samples (the box represents the typical platelet shape; the arrow represents the fibrin)

The complete DPP-sample direct contact hemolysis test results (Fig. 5b) show that the hemolysis rate of the OKGM-fixed samples is significantly lower than that of the GA-fixed and GNP-fixed samples, and the hemolysis rates of all samples are less than 5%. The hemolysis rate tested by the two methods met the clinical requirements for implants according to the international standard ISO 10993–4:2017(E).

Anticoagulation is an essential factor for the long-term patency of blood vessels [31]. Platelet adhesion and deposition are the leading causes of thrombosis and intimal hyperplasia. Therefore, inhibition of platelet adhesion on cardiovascular substitute materials is very important for small-diameter vascular grafts. Owing to the participation of GP Ib, vWF, and integrin $\alpha_{II}\beta_{3d}$, the adhesion of platelets onto the surface of cardiovascular substitute materials undergoes five processes (flowing-disc-shaped platelets, rolling ball-shaped platelets, hemisphere-shaped platelets, firm reversible adhesion, and spreading irreversible adhesion), and the platelet morphology undergoes corresponding changes during these processes. Among these processes, only the last step (spreading irreversible adhesion) is irreversible, which is conducive to capturing more proteins and platelets to adhere to the surface of the cardiovascular substitute materials, leading to platelet aggregation and thrombus formation of thrombi [32]. As observed by SEM (Fig. 5c), more flat platelets are spread irreversibly and aggregated on the DPP surface. There were many hemispherical platelets on the GA-fixed DPP, which were basically in the rolling ball-shape stage, on the GNP-fixed DPP, the platelets were slightly flat and their pseudopodia were more stretched, and most of them were in the hemisphere shape stage. The number of platelets adhering to OKGM-fixed DPP was significantly lower than that of the GA-fixed and GNP-fixed samples. Among these OKGM-fixed DPP, no platelets spread irreversibly on the surface of the 1:1.5 OKGM-fixed DPP. The results showed that OKGM-fixed DPP, especially 1:1.5 OKGM-fixed DPP, could significantly inhibit platelet adhesion.

The carotid artery in rabbits is thin and prone to thrombosis after puncturing owing to hemodynamic changes at the site of the puncture needle and cannula. In view of this, a semi-ex vivo circulation (Fig. 6a, b) was

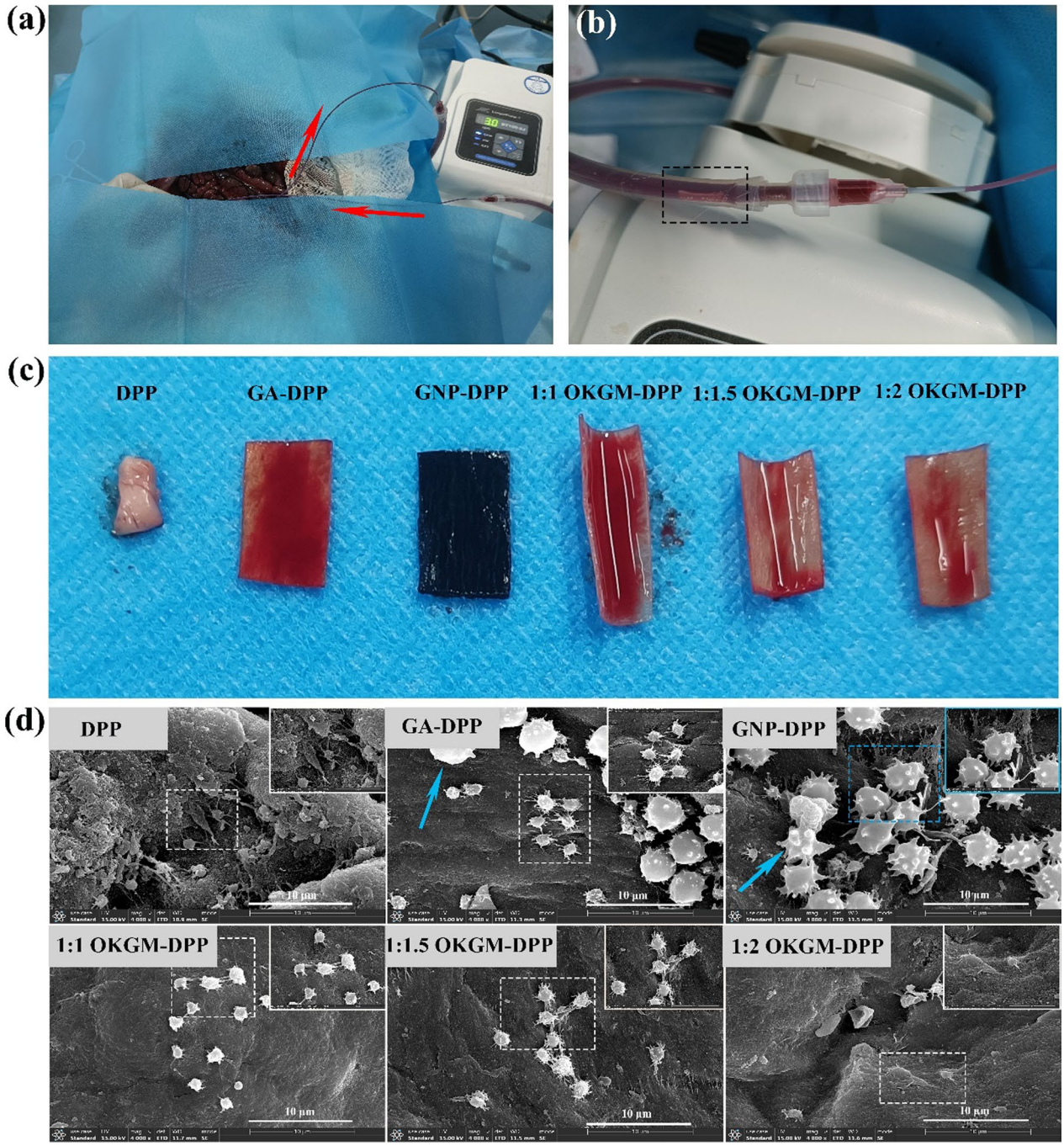

Fig. 6 Ex vivo blood contact test. **a** Abdominal aortic blood flow pathway (red arrows indicate the direction of arterial blood flow). **b** Sample sheet fixed to the inner wall of circulation pipe (black box indicates the location of sample). **c** Samples exposed to the flow of blood without heparin for 2 h. **d** SEM of sample surface. (White boxes indicate the typical platelets; blue arrow and blue boxes indicate the leukocyte)

constructed by ligating the abdominal aorta and cannulating the upper and lower ends of the vessel, and using a peristaltic pump to set the blood flow rate in vivo. The sheet sample was fixed to the inner surface of the blood circulation line, and arterial blood was extracted from rabbits for semi-ex vivo circulation to assess the anticoagulation properties and leukocyte adhesion of the sample. After circulation for 2 h, no thrombus is observed on the surface of the samples in each group (Fig. 6c). As shown in the SEM image (Fig. 6d), there are variable amounts

of adherent platelets without a fibrin network on the sample surface. Among them, more platelets are on the GA- and GNP-fixed DPP. In addition, a certain amount of leukocytes is also observed to adhere to their surfaces. The number of platelets adhering to the OKGM-fixed DPP was lower than that of the DPP, GA-, and GNP-fixed samples, and no leukocytes were found on their surfaces. This indicated a lower risk of thrombosis for OKGM-fixed DPP and also that GA- and GNP-fixed DPP might trigger a more severe inflammatory response. An important feature of the inflammatory response process in vessels is that leukocytes adhere to and infiltrate the vascular endothelium and engulf pathogens or tissue debris from exudation. Therefore, the amount of leukocyte adhesion and exudation could reflect the degree of inflammation [33]. At the site of vascular injury, excessive leukocyte adhesion needs to be avoided as excessive leukocyte adhesion and accumulation could lead to atherosclerosis [34]. Conversely, excessive leukocyte adhesion and infiltration is an important manifestations of vascular endothelial dysfunction [35]. Based on these results, the OKGM-fixed DPP, especially the 1:1.5 OKGM-fixed DPP, had better hemocompatibility.

3.6 In vitro anti-enzymatic hydrolysis of OKGM-fixed DPP

The main structural proteins in mammals are collagen and elastin, which provide mechanical support, strength, and elasticity in various tissues and organs. Collagen and elastin are readily available, biodegradable, biocompatible, and can stimulate cell growth [36]. In the anti-enzymatic hydrolysis experiments (collagenase I and collagenase IV) of fixed samples in vitro, the ability of GNP-fixed DPP to resist collagenase digestion is better than that of GA-fixed DPP at 72 h, and OKGM-fixed DPP is equivalent to GA-fixed DPP (Fig. 7). This indicates that GNP presents a better crosslinking effect on collagen than OKGM and GA, while OKGM and GA present the same crosslinking effect on collagen. Masson staining results (Additional file 1: Figs. S2–S3) show that the structure of collagen fiber in GNP-fixed DPP is well preserved. The same result was also observed for GA-fixed and 1:1.5 OKGM-fixed DPP.

Elastin keeps ECM in its original shape under stressful conditions. Elastin is mainly composed of hydrophobic amino acids [37]. Due to the lack of lysine residues as reactive groups, it is difficult to fix and stabilize natural elastin through covalent interactions. Therefore, the commercial crosslinker GA cannot effectively crosslink elastin. This conclusion was confirmed in the present research. The ability of GNP-fixed and OKGM-fixed DPP to resist elastase digestion was better than that of GA-fixed DPP and DPP alone. EVG staining results showed no obvious elastic fibers were observed in the GA-fixed DPP after 72 h of elastase-enzymolysis in vitro, and its microstructure was seriously damaged. The elastic fiber microstructure (Additional file 1: Fig. S4) in the 1:1.5 and 1:2 OKGM-fixed DPP samples was preserved as well as that of the GNP-fixed DPP. The results indicated that GA had a poor crosslinking effect on elastin and was unsuitable for crosslinking DPP. However, GNP had a good crosslinking effect on both collagen and elastin, and their resistance to enzymatic hydrolysis (collagenase and elastase) in vitro was the best. The crosslinking effect of OKGM on collagen and elastin was second only to that of GNP. It also demonstrated a good crosslinking effect on DPP.

3.7 In vitro calcification of OKGM-fixed DPP

The calcification process of the vessel and valve is similar to bone mineralization, and there are two main stages: calcium phosphate nucleation and further growth of crystals [38–40]. The initiation and progression of calcification depend on the microstructure of the biomaterials (including collagen fibers and elastic fibers). The low crosslinked elastin protein has large open spaces between molecules because of the lack of functional groups that will react with aldehydes and epoxy compounds. It has many calcium-binding sites that provide a central site for

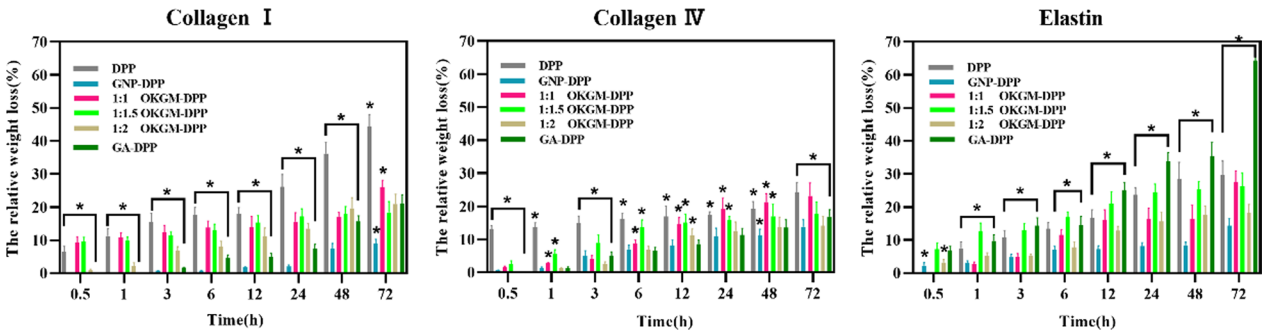

Fig. 7 Weight loss rate of fixed samples during enzymatic hydrolysis (*indicates significant difference compared to the GA-DPP group)

crystal nucleus formation. Therefore, the more elastin the biomaterials contain, the faster their calcification rates. As representative small-molecule crosslinking agents, GA and GNP are usually used to crosslink bovine pericardium to construct artificial heart valves. However, this artificial heart valve presents a serious risk of long-term calcification, which limits its long-term implantation. Grafts fixed by other crosslinking agents (including EDC, ethylene oxide, proanthocyanidins, sodium alginate, etc.) also demonstrated serious instances of calcification either in vitro or in vivo, causing implantation failure [41]. We developed a novel OKGM to crosslink DPP and detected the calcification of OKGM-fixed DPP in vitro through EDS (Fig. 8a) and SEM (Fig. 8b). DPP exhibited the maximum degree of calcification, and its calcium content reached more than 30% after incubation for 60 and 90 days. The calcium content of GA-fixed and GNP-fixed DPP was approximately 1% after incubation for 60 and 90 days. The OKGM-fixed DPP presented the lowest degree of calcification because of its smooth surface with almost no calcium deposits. The results suggested that OKGM-fixed DPP had significantly better anti-calcification capability in vitro than GA-fixed and GNP-fixed DPP. Although OKGM does not wholly prevent the first stage of calcification in the peritoneum, it can delay the mineralization of elastin and reduce the second stage of calcification. However, the underlying mechanism remains unclear. We speculate that one of the reasons for this is that OKGM can simultaneously crosslink collagen and elastin.

3.8 The mechanical properties of OKGM-fixed DPP

Adequate mechanical properties are essential for cardiovascular materials, particularly for artificial heart valves and small-diameter vascular grafts [42]. According to the literature, the axial E-modulus of a 6 mm aorta is 9.13 MPa, and the ultimate tensile stress is 4.03 MPa [43–45]. Uniaxial tensile testing (Fig. 9) is one of the most commonly used methods for measuring the mechanical properties of cardiovascular materials. The ultimate tensile stress (Fig. 9a, b) of OKGM-fixed DPP is 3.43 MPa, which is slightly lower than that of the artery, GA-fixed DPP and GNP-fixed DPP, but there is no significant difference in the ultimate tensile stress among them. Conversely, the E-modulus of OKGM-fixed DPP (Fig. 9c) is 12 MPa, which is slightly higher than that of the artery, GA-fixed DPP and GNP-fixed DPP. However, there was still no significant difference in the E modulus among them.

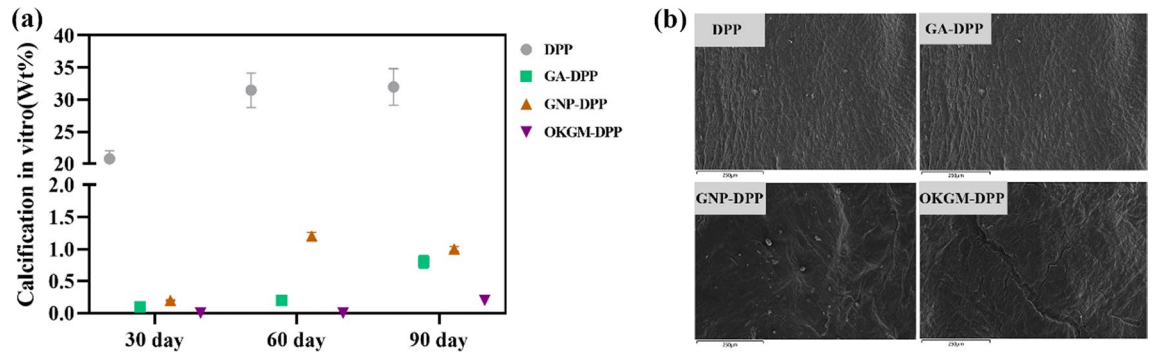

Fig. 8 In vitro calcification detected by **a** EDS and **b** SEM (OKGM-DPP indicate the 1:1.5 OKGM-fixed DPP)

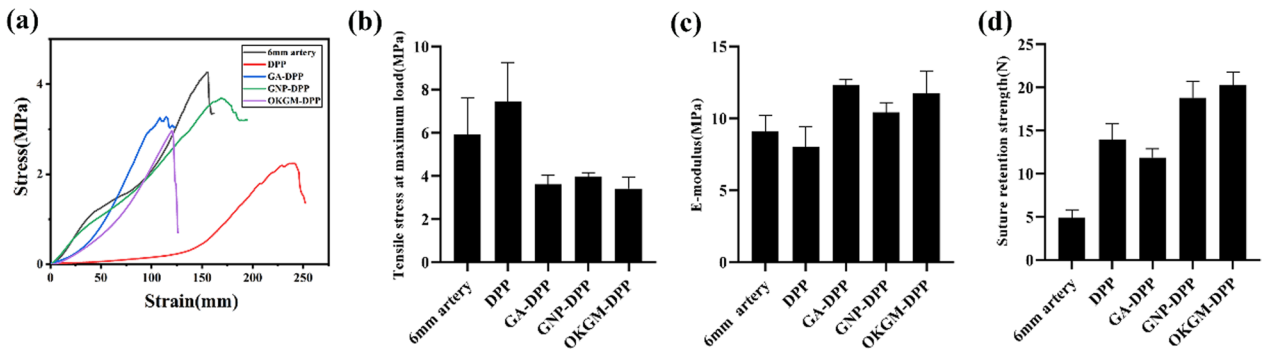

Fig. 9 The mechanical properties of crosslinked DPP. a Stress-strain curves. b Tensile stress at maxiun load(MPa). c E-modulus(MPa). d Suture retention strength(N)

Vascular grafts require a certain suture retention strength to ensure clinical use, and the demand for suture retention strength of vascular grafts is at least 1 N. The suture retention strength results for various samples are shown in Fig. 9d. The suture retention strength of GA-fixed DPP and GNP-fixed DPP was significantly higher than that of the 6 mm artery and OKGM-fixed DPP. Furthermore, OKGM-fixed DPP had an equivalent suture retention strength to that of the 6 mm artery, which was approximately 7.9–9.2 N. In fact, suture retention strength that is too high is not conducive to anastomosis. The above results confirm that the mechanical properties of the OKGM-fixed DPP is the nearest to the human artery, meeting the mechanical performance requirements for vascular grafts.

3.9 Degradation and inflammation of OKGM-fixed DPP in vivo

A subcutaneous implantation model of the SD rat subjects for 90 days was used to investigate the biocompatibility of the samples. As shown in Fig. 10a, compared with OKGM-fixed DPP, there are more blood vessels around the DPP and GA-fixed DPP/GNP-fixed DPP 12 weeks after subcutaneous implantation. This demonstrated that the inflammation caused by DPP, GA-fixed DPP, and GNP-fixed DPP was still obvious, and the sample morphologies showed noticeable changes due to degradation in vivo. The morphology of the GNP-fixed DPP and OKGM-fixed DPP remained relatively complete. No apparent morphological changes due to degradation and no obvious inflammation were observed in the OKGM-fixed samples, indicating their good histocompatibility. Samples were retrieved from the subdermal sites for histological analysis. HE staining results showed (Fig. 10b) that DPP presented more fiber breakage in vivo and more inflammatory cell infiltration compared with samples in other groups. GA-fixed DPP and GNP-fixed DPP maintained better fiber morphology because of their ability to resist enzymatic digestion, but inflammatory cell infiltration in these samples was also high, indicating serious inflammation. OKGM-fixed DPP presented fewer broken fibers,

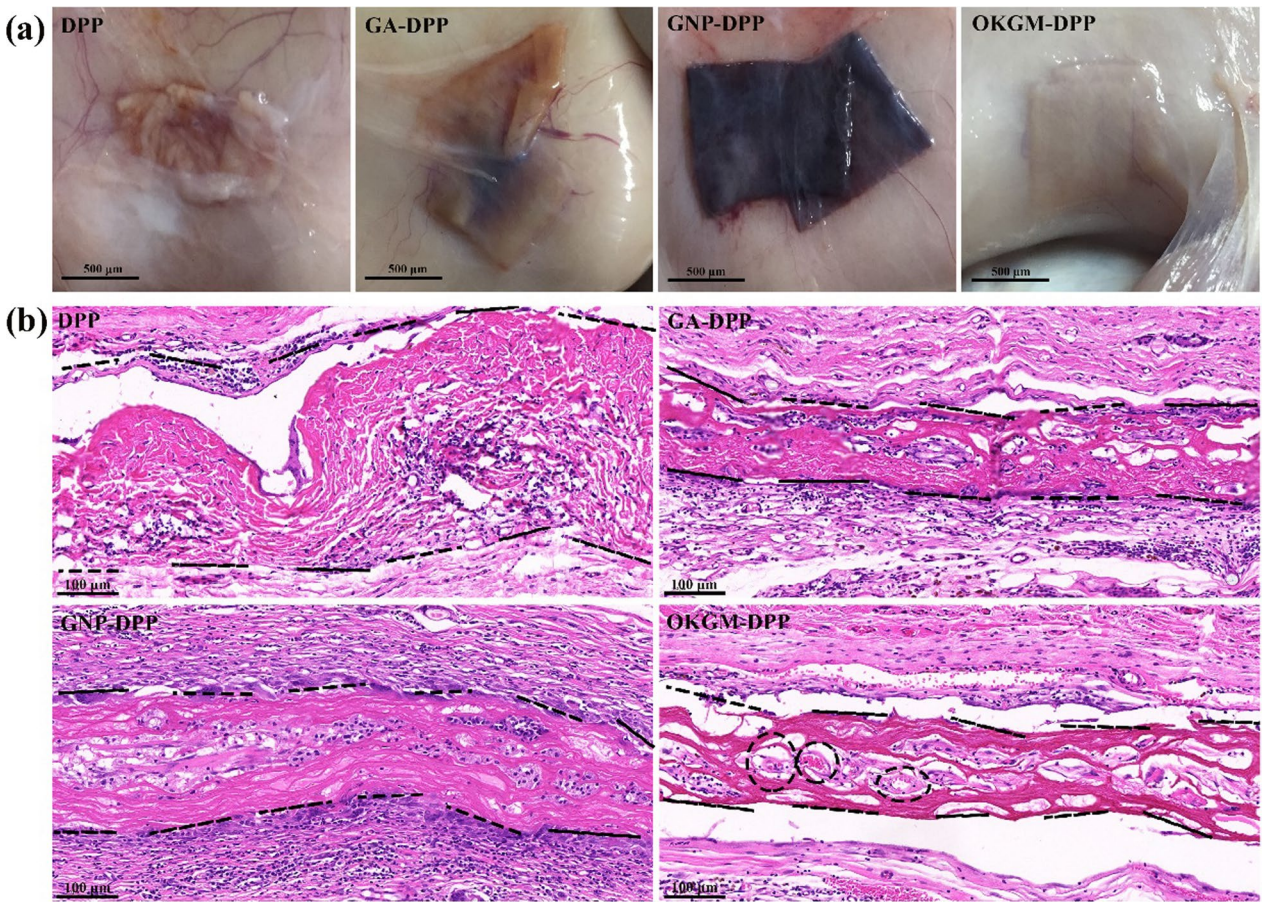

Fig. 10 Sample morphology (**a**) and inflammatory cell infiltration (**b**) after 12 weeks of subcutaneous implantation (black curve indicates sample edge; black circles indicate neovascularization)

and its shape retention was second only to GNP-fixed DPP. It is to be noted that there was no inflammatory cell infiltration observed in the sample, while massive neovascularization around the sample was found. This indicated that OKGM-fixed DPP had good histocompatibility in vivo, which was beneficial to the migration of endothelial cells, and thus could promote angiogenesis in implants in vivo.

4 Conclusion

The peritoneum is a thin elastic membrane. After decellularization, DPP is a promising animal-derived biomaterial that remains intact ECM and suitable mechanical properties. In this research, $NaIO_4$ was applied to oxidize KGM to prepare a polysaccharide crosslinker, OKGM, and then used OKGM to stablize DPP to prepare a novel cardiovascular substitute material. For the preparation of OKGM, the results showed that OKGM obtained using a feeding ratio of 1:1.5 (KGM:$NaIO_4$) possessed an appropriate molecular weight and degree of oxidation, with almost no cytotoxicity. Furthermore, 3.75% OKGM [1:1.5 (KGM:$NaIO_4$)] was used as a cross-linking agent to fix DPP to prepare a cardiovascular substitute material and the prepared material exhibited good cross-linking characteristics. Compared to GA-fixed DPP and GNP-fixed DPP, this novel 3.75% OKGM-fixed DPP exhibited suitable mechanical strength, excellent HEVC-cytocompatibility, hemocompatibility, anti-calcification capability, and resistance to enzymatic degradation in vitro, as a cardiovascular substitute material. It also exhibits good histocompatibility in vivo. This research provides an experimental basis for OKGM as a new cross-linking reagent for fixing natural tissues featured with rich collagen content and 3.75% OKGM-fixed DPP as a potential cardiovascular substitute material.

Supplementary Information

The online version contains supplementary material available at https://doi.org/10.1186/s42825-023-00114-w.

Additional file 1. Fig.S1. Morphology of peritoneum. **Fig.S2.** Masson staining of samples hydrolyzed by collagenase I. **Fig.S3.** Masson staining of samples hydrolyzed by collagenase IV. **Fig.S4.** EVG staining of samples hydrolyzed by elastase.

Acknowledgements
We would be grateful to the help of Xiaomei Zhang from Experimental and Research Animal Institute, Sichuan University, for providing the fresh porcine peritoneum and raising animals.

Author contributions
XP: experiment, analysis, and writing. LL and CC: experiment, editing. JX: analysis and editing. MH, YL, SS: experiment, editing. YL and ZC: Preparation and staining of pathological tissues. XY: funding acquisition, review, and editing. All authors read and approved the final manuscript.

Funding
This work was financially supported by National Key Research and Development Program of China [Nos. 2016YFC1100900, 2016YFC1100901, 2016YFC1100903 and 2016YFC1100904]. "From 0 to 1" innovative research projects of Sichuan University (2022SCUH0045). The Key Research and Development Program of Sichuan Province (2020YFS0278).

Availability of data and materials
All data from this research are presented in the paper and the supplementary material.

Declarations

Ethics approval and consent to participate
All animal experiments were conducted in compliance with the guidelines of the Administration Committee of Experimental Animals in Sichuan Province and the Animal Care Committee of Sichuan University (No. K2021036). Male SD Rat (220 ± 10 g) and New Zealand rabbit (3 kg) were purchased from Experimental and Research Animal Institute, Sichuan University.

Competing interests
The authors declare no conflict of interest.

Author details
[1]College of Polymer Science and Engineering, Sichuan University, Chengdu 610065, People's Republic of China. [2]Experimental and Research Animal Institute, Sichuan University, Chengdu 610065, People's Republic of China. [3]Department of Oncology Hematology, Western Theater Command Air Force Hospital, Chengdu 610021, People's Republic of China. [4]Max Planck Institute for Polymer Research, 55128 Mainz, Germany. [5]Department of Growth and Reproduction, Copenhagen University, Copenhagen, Denmark.

Received: 9 October 2022 Revised: 31 December 2022 Accepted: 5 January 2023
Published online: 10 February 2023

References

1. Hurt AV, Batello-Cruz M, Skipper BJ, et al. Bovine carotid artery heterografts versus polytetrafluoroethylene grafts. A prospective, randomized study. Am J Surg. 1983;146(6):844–7.
2. Schmidli J, Savolainen H, Heller G, et al. Bovine mesenteric vein graft (ProCol) in critical limb ischaemia with tissue loss and infection. Eur J Vasc Endovasc Surg. 2004;27(3):251–3.
3. Kovalic AJ, Beatti DK, Davies AH. Outcome of ProCol, a bovine mesenteric vein graft, in infrainguinal reconstruction. Eur J Vasc Endovasc Surg. 2002;24(6):533–4.
4. Cheml ES, Morsy M. Randomized clinical trial comparing decellularized bovine ureter with expanded polytetrafluoroethylene for vascular access. Br J Surg. 2009;96(1):34–9.
5. Waterhouse A, Wise SG, Ng Martin KC, et al. Elastin as a nonthrombogenic biomaterial. Tissue Eng B Rev. 2011;17(2):93–9.
6. Patel A, Fine B, Sandig M, et al. Elastin biosynthesis: the missing link in tissue-engineered blood vessels. Cardiovasc Res. 2006;71(1):40–9.
7. Wang Z, Liu L, Mithieux SM, et al. Fabricating organized elastin in vascular grafts. Trends Biotechnol. 2021;39(5):505–18.
8. de Torre IG, Alonso M, Rodriguez-Cabello J-C. Elastin-based materials: promising candidates for cardiac tissue regeneration. Front Bioeng Biotechnol. 2020;8:657.
9. Delgado LM, Bayon Y, Pandit A, et al. To cross-link or not to cross-link? Cross-linking associated foreign body response of collagen-based devices. Tissue Eng B Rev. 2015;21(3):298–313.
10. Lei Y, Guo G, Wanyu Y, et al. Riboflavin photo-cross-linking method for improving elastin stability and reducing calcification in bioprosthetic heart valves. Xenotransplantation. 2019;26(2):e12481.
11. Sung HW, et al. Stability of a biological tissue fixed with a naturally occurring crosslinking agent (genipin). J Biomed Mater Res. 2001;55(4):538–46.

12. Yu H, Lu J, Xiao C. Preparation and properties of novel hydrogels from oxidized konjac glucomannan cross-linked chitosan for in vitro drug delivery. Macromol Biosci. 2007;7(9–10):1100–11.
13. Liu J, Li J, Yu F, et al. In situ forming hydrogel of natural polysaccharides through Schiff base reaction for soft tissue adhesive and hemostasis. Int J Biol Macromol. 2020;147:653–66.
14. Liao Z, Wang Y, Hongxia W. Effects of Oxidized Konjac glucomannan (OKGM) on growth and immune function of *Schizothorax prenanti*. Fish Shellfish Immunol. 2013;35(4):1105–10.
15. Bax DV, Davidenko N, Gullberg D, et al. Fundamental insight into the effect of carbodiimide crosslinking on cellular recognition of collagen-based scaffolds. Acta Biomater. 2017;49:218–34.
16. Takigawa TE, et al. Effects of glutaraldehyde exposure on human health. J Occup Health. 2006;48(2):75–87.
17. Cossarizza A. Guidelines for the use of flow cytometry and cell sorting in immunological studies. Eur J Immunol. 2017;47(10):1584–797.
18. Joziasse DH, Oriol R. Xenotransplantation: the importance of the Galalpha 1,3Gal epitope in hyperacute vascular rejection. Biochim Biophys Acta. 1999;1455(2–3):403–18.
19. Orlando G, Remuzzi G, Williams DF, et al. Chapter 84-Xenotransplantation and kidney regenerative technology. In: Kidney transplantation, bioengineering and regeneration. Academic Press; 2017. p. 1151–61.
20. Chen L, Allison D, Frank D, et al. Smooth muscle-alpha actin inhibits vascular smooth muscle cell proliferation and migration by inhibiting RAC1 activity. PLoS ONE. 2016;11(5):e0155726.
21. Lisha Gu, Shan T, Ma Y-X, et al. Novel biomedical DPPlications of crosslinked collagen. Trends Biotechnol. 2019;37(5):464–91.
22. Blackburn SC, Stanton MP. Anatomy and physiology of the peritoneum. Semin Pediatr Surg. 2014;23(6):326–30.
23. Schaefer B, Bartosova M, Macher-Goeppinger S, et al. Quantitative histomorphometry of the healthy peritoneum. Sci Rep. 2016;6:21344.
24. Huang LL, Hsing WS, Chen CT, et al. Biocompatibility study of a biological tissue fixed with a naturally occurring crosslinking reagent. J Biomed Mater Res. 1998;42(4):568–76.
25. Liang HC, Chang Y, Hsu CK, et al. Effects of crosslinking degree of an acellular biological tissue on its tissue regeneration pattern. Biomaterials. 2004;25(17):3541–52.
26. Langer R. Selected advances in drug delivery and tissue engineering. J Control Release. 1999;62(1–2):7–11.
27. Wang Y, Siyuan C, Yiwa P, et al. Rapid in situ endothelialization of a small diameter vascular graft with catalytic nitric oxide generation and promoted endothelial cell adhesion. J Mater Chem B. 2015;3(47):9212–22.
28. Alkharsah KR, Singh VV, Bosco R, et al. Deletion of Kaposi's sarcoma-associated herpesvirus FLICE inhibitory protein, vFLIP, from the viral genome compromises the activation of STAT1-responsive cellular genes and spindle cell formation in endothelial cells. J Virol. 2011;85(19):10375–88.
29. Onoe H, Okitsu T, Itou A, et al. Metre-long cell-laden microfibres exhibit tissue morphologies and functions. Nat Mater. 2013;12(6):584–90.
30. Weber M, Steinle H, Golombek S, et al. Blood-contacting biomaterials: in vitro evaluation of the hemocompatibility. Front Bioeng Biotechnol. 2018;6:99.
31. Zheng W, Wang Z, Song L, et al. Endothelialization and patency of RGD-functionalized vascular grafts in a rabbit carotid artery model. Biomaterials. 2012;33(10):2880–91.
32. Kuwahara M, Sugimoto M, Tsuji S, et al. Platelet shape changes and adhesion under high shear flow. Arterioscler Thromb Vasc Biol. 2002;22(2):329–34.
33. Freire M, Van Dyke TE. Natural resolution of inflammation. Periodontol. 2013;63(1):149–64.
34. Mauersberger C, Hinterdobler J, Schunkert H, et al. Where the action is-leukocyte recruitment in atherosclerosis. Front Cardiovasc Med. 2021;8:813984.
35. Thijs J, Sluiter JD, et al. Endothelial barrier function and leukocyte transmigration in atherosclerosis. Biomedicines. 2021;9(4):328.
36. Skopinska W, Wegrzynowska K, Bajek A, et al. Is dialdehyde starch a valuable cross-linking agent for collagen/elastin based materials? J Mater Sci Mater Med. 2016;27(4):67.
37. Christoph US, Heinz A, Majovsky P, et al. Elastin is heterogeneously cross-linked. J Biol Chem. 2018;93(39):15107–19.
38. Badria AF, Koutsoukos Dimosthenis PG. Decellularized tissue-engineered heart valves calcification: what do animal and clinical studies tell us? J Mater Sci Mater Med. 2020;31(12):132.
39. Leopold JA. Cellular mechanisms of aortic valve calcification. Circ Cardiovasc Interv. 2012;5(4):605–14.
40. Zhai W, Jiang C, Lin K, et al. Crosslinking of decellularized porcine heart valve matrix by procyanidins. Biomaterials. 2006;27(19):3684–90.
41. Ma B, Wang X, Wu C, et al. Crosslinking strategies for preparation of extracellular matrix-derived cardiovascular scaffolds. Regen Biomater. 2014;1(1):81–9.
42. Wang D, Xu Y, Li Q, et al. Artificial small-diameter blood vessels: materials, fabrication, surface modification, mechanical properties, and bioactive functionalities. J Mater Chem B. 2020;8(9):1801–22.
43. Gerhardt K, Todd NM, Nathalie D, et al. Mechanical properties of completely autologous human tissue engineered blood vessels compared to human saphenous vein and mammary artery. Biomaterials. 2009;30(8):1542–50.
44. Vivek AK, Luke PB, Jeffrey MC, et al. Tissue engineering of blood vessels: functional requirements, progress, and future challenges. Cardiovasc Eng Technol. 2011;2(3):137–48.
45. Lillie MA, Shadwick RE, Gosline JM. Mechanical anisotropy of inflated elastic tissue from the pig aorta. J Biomech. 2010;43(11):2070–8.

Publisher's Note